IEEE Access
Multidisciplinary | Rapid Review | Open Access Journal

Received April 21, 2020, accepted April 29, 2020, date of publication May 4, 2020, date of current version May 18, 2020.

Digital Object Identifier 10.1109/ACCESS.2020.2992129

A Modified Sequential Multiplexed Method for Detecting Airborne and Sea Targets With Over-the-Horizon Radar

ZHAOYI WANG, SHENGNAN SHI, ZIYANG CHENG, AND ZISHU HE, (Member, IEEE)
School of Information and Communication Engineering, University of Electronic Science and Technology of China, Chengdu 611731, China

Corresponding author: Ziyang Cheng (zeeyoungcheng@163.com)

This work was supported by the National Natural Science Foundation of China under Grants 61671139 and 61871102.

ABSTRACT Phased array over-the-horizon (OTH) radar usually needs to detect sea target and airborne target in different directions. Conventionally, the sea target and airborne target are detected sequentially with the coherent integration completely accomplished for each of them. However, the long coherent integration time (CIT) required by the sea target makes the time interval between two airborne target detections too long, which is not conducive to tracking airborne target. To overcome this problem, this paper proposes a new timeframe multiplexing scheme, in which several short-time detections of airborne target are inserted into a long CIT of sea target detection. The proposed scheme seeks to improve the detection frequency of airborne target while ensuring the detection performance of two types of target. However, due to the insertion of airborne target detection, the echo from sea surface is received discontinuously which means that the coherent integration of sea target is incomplete. To tackle it, a recovery algorithm based on the Hankel structured matrix is introduced, which recovers the slow-time domain signal of each range bin and thereby guarantees the detection performance of sea target not damaged. Numerical simulations prove the effectiveness of the proposed algorithm for signal recovery, and also verify that the proposed operating scheme has a shorter time interval for airborne target detection, while the detection performance of two targets are well guaranteed.

INDEX TERMS OTH radar, multi-target detection, timeframe multiplexed, matrix recovery, Hankel structure constraint.

I. INTRODUCTION

High-frequency sky-wave over-the-horizon (OTH) radar can monitor a broad area via ionospheric reflection [1]–[3]. It is a very common requirement for OTH radar to monitor the sea surface and airspace simultaneously, and generally the aircraft and ship are most concerned by the radar for early warning. For multi-target detection, one of the methods is to form a multi-beam transmit beam-pattern to achieve concurrent detection [4], [5]. However, to detect aircraft in airspace and to detect ship on sea surface, the pulse repetition interval (PRI) of the transmit waveform and the coherent integration time (CIT) are different, due to the different characteristics of environments and targets [6]–[8]. Therefore, the concurrent detection, which detects different targets using the same configuration of PRI and CIT, is not suitable in this scenario. That is to say, the OTH radar has to scan the sea surface and airspace alternatively, and therefore the detections to different targets are processed sequentially.

To perform sequential detection, the radar conventionally finishes a complete coherent integration of sea target detection, before changing the beamforming direction for airborne target detection. Considering that a long CIT of 30sec-100sec is usually required for sea target detection to achieve a high Doppler resolution to separate the sea target from the strong sea clutter, there will be a long time interval between two adjacent detections of airborne target. This is undesirable since the airborne target usually move at high speed and long detection interval can cause trouble for tracking. To overcome this shortage, some works resort to shorten the CIT of sea target detection [9]–[12], with the modern spectrum estimation method [9], [10] or high accuracy parameter estimation method [11] used to compensate the Doppler loss caused by the short CIT. However, due to the short CIT, the

The associate editor coordinating the review of this manuscript and approving it for publication was Wei Wang.

information contained in the echo is limited, and the performance of the above estimation methods can be affected by many factors. For example, the time-varying characteristics of the ionosphere.

In this paper, we engage a novel operating scheme for OTH radar simultaneously detecting the sea target and airborne target. To reduce the time interval of airborne target detection, we are not committed to shortening the CIT of sea target detection within the framework of conventional scheme, but attempt to insert several airborne target detections into a long CIT of sea target detection. However, due to the insertion of airborne target detection, the coherent integration of sea target detection is incomplete, i.e., several pulses in sea surface echo are missed. Fortunately, the coherence of sea surface echo can be maintained as long as we can recover the data in those missing pulses.

Assume that M_s pulses are received in a CIT of ship detection. After pulse compression, the sea surface echo of M_s pulses from a certain range bin is compressed into an $M_s \times 1$ vector, which is denoted as $\boldsymbol{r}$ and is referred as slow-time domain signal [13, Section 4.2.1]. Due to the absence of some pulses, the corresponding elements in $\boldsymbol{r}$ are vacant. Hence, in order to maintain the detection performance of ship, the key problem is to recover the missing element in $\boldsymbol{r}$. Inspired by the matrix recovery techniques [13]–[17], we first organize $\boldsymbol{r}$ into a Hankel matrix, which can be proven to be low rank [18]. Then, a low-rank matrix recovery problem is proposed, which involves Hankel structure constraint to ensure that its solution is also a Hankel matrix. Thereby, a vector can be extracted from the obtained matrix, which is regarded as the recovered signal of $\boldsymbol{r}$. Also, an iterative algorithm is developed, which extends the Inexact Augmented Lagrange Multiplier (IALM) [19] method and is capable of solving the proposed problem with Hankel structure constraint.

The main contents and contributions of this article are summarized as follows.

(1) A new operating scheme is developed for OTH radar to detect airborne target and sea target in different directions. The proposed schemes can improve the data update rate of airborne target detection, while maintaining the detection performance of two types of target. In addition, it can be implemented on the current hardware equipment, with mature technology, i.e., digital beamforming.

(2) An iterative algorithm is developed to recover the incomplete slow-time domain signal of sea surface echo (i.e., $\boldsymbol{r}$). The proposed algorithm extends the IALM method to involve Hankel constraint and recovers $\boldsymbol{r}$ based on the basis of Hankel matrix.

(3) Simulation experiments show that the proposed algorithm can effectively recover the incomplete slow-time domain signal of sea surface. Moreover, the sea target detection performance based on the recovered data is evaluated, regarding the main-to-side lobe ratio and peak-to-average ratio after clutter suppression filter.

The remainder of this paper is organized as follows. A brief introduction to the conventional sequential detection scheme is given in Sec.II. The proposed operating scheme is introduced in Sec.III and Sec.IV. Numerical simulations are illustrated in Sec.IV. And the conclusion is drawn in Sec.V.

TABLE 1. Parameters of transmitter for different types of targets.

Target type	sea target	airborne target
Beamforming direction	θ_1	θ_2
Number of pulses within a CIT	M_s	M_a
Pulse repetition interval	T_s	T_a
Coherent integration time	$\mathrm{CIT}^{(s)}$	$\mathrm{CIT}^{(s)}$

[1] Usually, T_a is much smaller than T_s, and M_a can be half or quarter of M_s. Moreover, $\mathrm{CIT}^{(a)}$ is about $\frac{1}{40}\sim\frac{1}{20}$ of $\mathrm{CIT}^{(s)}$.

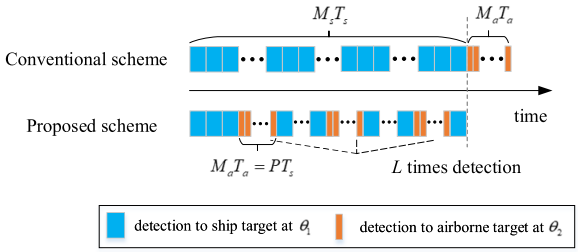

FIGURE 1. Conventional operating scheme and proposed operating scheme for OTH radar.

Notations: Throughout this paper, the italic letters indicate scalars, the bold italic lowercase letters are used to represent vectors, and bold italic uppercase letters signify matrices. $N \times N$ complex space is denoted by $\mathbb{C}^{N\times N}$. $\{\cdot\}^H$, $\{\cdot\}^*$ and $\{\cdot\}^T$ denote the operations of complex conjugate transpose, conjugate, and transpose, respectively. tr$(\cdot)$ represents the matrix trace and $\langle \boldsymbol{A}, \boldsymbol{B}\rangle$ is the inner product of $\boldsymbol{A}$ and $\boldsymbol{B}$. $\|\cdot\|_F$ is the Frobenius norm and $\|\cdot\|_*$ denotes the nuclear norm of a matrix. svd$(\cdot)$ means the singular value decomposition. $\boldsymbol{x}[m]$ denotes the m-th element of the vector $\boldsymbol{x}$ and $[\boldsymbol{X}]_{i,j}$ denotes the (i, j)-th element of the matrix $\boldsymbol{X}$. $\boldsymbol{I}_n$ represents a $n\times n$ identity matrix and $\boldsymbol{0}_{n_1\times n_2}$ represents a $n_1\times n_2$ matrix with all elements equal to zero.

II. CONVENTIONAL OPERATING SCHEME AND SIGNAL MODEL

A. CONVENTIONAL OPERATING SCHEME

Denoting the PRI as T and the number of pulses within a CIT as M, the transmitted waveform can be expressed as

$$x(t) = e^{j2\pi f_0 t} \sum_{m=1}^{M} x_0(t - mT)\,\mathrm{rect}\left(\frac{t - mT}{T}\right), \qquad (1)$$

where f_0 is the operating frequency. $x_0(t)$ is baseband transmitted pulse, which should have good pulse compression property, e.g., the linear frequency modulation (LFM) waveform. However, when the radar detects different types of targets, the settings of M and T are different. To ease the discussion, Table 1 details the definitions of the parameters involved in the following discussion.

The conventional operating scheme is illustrated in Fig.1.

As shown in the figure, the radar first focuses on the direction θ_1 to detect sea target, consuming $\mathrm{CIT}^{(\mathrm{s})} = M_s T_s$ for the coherent integration. Then, the radar changes the beamforming direction to θ_2 and spends $\mathrm{CIT}^{(\mathrm{a})} = M_a T_a$ for coherent integration.

B. SIGNAL MODEL FOR CONVENTIONAL SCHEME

In this section, we briefly illustrate the formulations of received signal from sea surface for the conventional scheme. For details of related theory and formula derivation, interested readers can refer to [20].

At the receiving end, the carrier frequency of the echo (including M_s pulses) is first removed. Then, after beamforming in direction θ_1, we obtain an $M_s N \times 1$ vector, where N is the number of samples in one PRI. The $M_s N \times 1$ vector is next processed by matched filter and phase compensation. After that, echoes with different time-delays (or in other word, from different range bins) can be separated and each of them is compressed into an $M_s \times 1$ vector. As a consequence, we can arrange a matrix $\boldsymbol{D}_s = [\boldsymbol{s}_1, \ldots, \boldsymbol{s}_n, \ldots, \boldsymbol{s}_N] \in \mathbb{C}^{M_s \times N}$. In matrix $\boldsymbol{D}_s$, the n-th column vector ($\boldsymbol{s}_n$) is called as the slow-time domain signal of the n-th range bin [20, Section 4.2]. More specifically, $\boldsymbol{s}_n$ is the pulse compression result of the echo from the n-th range bin, and the m-th element in $\boldsymbol{s}_n$ (i.e., $\boldsymbol{s}_n[\mathrm{m}]$) represents the data received from n-th range bin in m-th pulse. Further signal processing such as clutter suppression and target detection will be performed on each $\boldsymbol{s}_n$.

In the following, we omit the subscript n of $\boldsymbol{s}_n$, using $\boldsymbol{s}$ to broadly represent the slow-time domain signal of a range bin. Depending on whether the target exists, $\boldsymbol{s}$ can be formulated as follows

$$\boldsymbol{s} = \begin{cases} \boldsymbol{u} + \boldsymbol{c} + \boldsymbol{n}\,, & \text{if the target exists,} \\ \boldsymbol{c} + \boldsymbol{n}\,, & \text{otherwise,} \end{cases} \tag{2}$$

where $\boldsymbol{u} \in \mathbb{C}^{M_s \times 1}$ and $\boldsymbol{c} \in \mathbb{C}^{M_s \times 1}$ are respectively the slow-time domain signals of the target echo and the sea clutter echo. $\boldsymbol{n} \in \mathbb{C}^{M_s \times 1}$ is the slow-time domain signal of environmental noise. Usually, the noise can be modeled as white Gaussian noise with zero mean.

In the following, the formulations of $\boldsymbol{u}$ and $\boldsymbol{c}$ are derived, based on the several general assumptions [21]:

(1) In radar illuminating region, there is a sea target moving at a constant speed. That is, its Doppler frequency is a constant and the its Doppler rate is zero. In addition, its speed is relatively slow, so that its movement dose not cross the range bin during a $\mathrm{CIT}^{(\mathrm{s})}$.

(3) The ionospheric phase contamination can be completely corrected by phase compensation.

(4) The sea state is unchanged during a $\mathrm{CIT}^{(\mathrm{s})}$.

Generally, for a target moving at a constant speed, its echo (in baseband) can be modeled as follows [22], [23]:

$$y_u(t) = b \sum_{m=1}^{M_s} x_0(t - mT_s - \tau) e^{j(2\pi f_d t + \phi)} \tag{3}$$

where b is a complex coefficient associating with the propagation loss and initial phase. τ is time delay and f_d is the Doppler frequency of the target. ϕ is the phase shift due to ionospheric phase contamination.

After pulse compression and phase compensation, the corresponding slow-time domain signal (i.e., $\boldsymbol{u}$), can be equivalently expressed as:

$$\boldsymbol{u} = b[1,\, e^{j2\pi f_d T_s}, \ldots, e^{j2\pi f_d (M_s - 1) T_s}]^T. \tag{4}$$

The detailed derivation from (3) to (4) can refer to [20, Equations (4.36)-(4.42)].

Sea clutter is composed of echoes backscattered by a large number of ocean waves. According to Bragg scattering hypothesis [24], [25], there are two ocean waves moving with specific direction and speed can strongly scatter the radar wave, composing the main component of the sea clutter. Based on this, the sea clutter echo can be formulated as:

$$\begin{aligned} y_c(t) = a_1 \sum_{m=1}^{M_s} x_0(t - mT_s) e^{j(2\pi f_B t + \phi)} \\ + a_2 \sum_{m=1}^{M_s} x_0(t - mT_s) e^{-j(2\pi f_B t + \phi)} + y_{\bar{c}}(t) \end{aligned} \tag{5}$$

where $f_B = \sqrt{g f_0 / \pi c}$ is called as Bragg frequency. $y_{\bar{c}}(t)$ stands for the other components in $y_c(t)$. a_1, a_2 and a_3 are the complex coefficients, with a_3 much smaller than a_1 and a_2. Based on (5) and following with [26, Equations (6)-(8)], the slow-time domain signal $\boldsymbol{c}$ can be given as follows:

$$\begin{aligned} \boldsymbol{c} = a_1 [1,\, e^{j2\pi f_B T_s}, \ldots, e^{j2\pi f_B (M_s - 1) T_s}]^T \\ + a_2 [1,\, e^{-j2\pi f_B T_s}, \ldots, e^{-j2\pi f_B (M_s - 1) T_s}]^T + a_3 \bar{\boldsymbol{c}}, \end{aligned} \tag{6}$$

where $\bar{\boldsymbol{c}} \in \mathbb{C}^{M_s \times 1}$ is the slow-time domain signal of $y_{\bar{c}}(t)$.

III. PROPOSED OPERATING SCHEME AND SIGNAL MODEL

A. PROPOSED OPERATING SCHEME

According to the above discussion, the conventional scheme takes the time of $\mathrm{CIT}^{(\mathrm{a})} + \mathrm{CIT}^{(\mathrm{s})}$ to sequentially complete a sea target detection and an airborne target detection. In this section, we try to develop a new operation scheme for OTH radar, which has also been illustrated in Fig.1. Three key points of the proposed scheme are concludes as follows.

(1) L detections of airborne target are inserted into a coherent detection of sea target. By doing so, the proposed scheme seeks to complete one detection to sea target and L times of detection to airborne target within the time of $\mathrm{CIT}^{(\mathrm{s})}$.

(2) Comparing with the traditional scheme, the time interval for radar detecting airborne target is significantly reduced. This is very attractive, since the airborne target usually moves fast and a long-time interval between two detections is not suitable for tracking.

(3) In the proposed scheme, each inserted airborne target detection has a complete coherent integration, so there is no impact on the airborne target detection performance. However, the coherent integration of the sea surface echo is

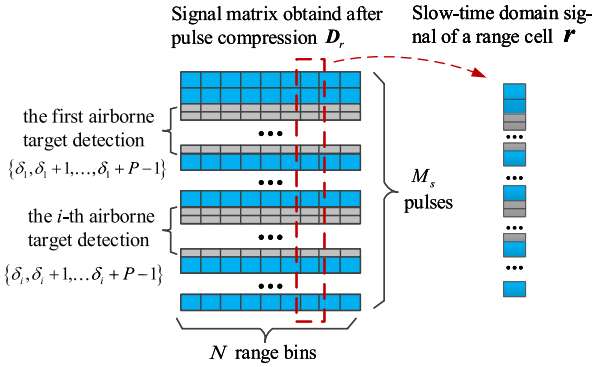

FIGURE 2. Illustration of signal matrix D_r and slow-time domain signal r.

interrupted. More specifically, each time the airborne target detection is inserted, the radar will miss the sea surface echo of P pulses, where $P = \mathrm{CIT}^{(a)}/T_s$. We denote that M_a, T_a and T_s can be carefully selected to satisfy that P is an integer.

Based on the above discussion, it is necessary to tackle the incomplete coherent integration of the sea surface echo so that the sea target detection performance is not lost. In the following, we first develop the signal model for the case of incomplete coherent integration. Then, we introduce how to complete the missing data.

B. SIGNAL MODEL FOR PROPOSED SCHEME

Now, we consider the received signal from sea surface for the proposed scheme. As we have discussed, the radar dose not have a complete echo signal of M_s pulses now. After pulse compression and other necessary operations, the incomplete echo is arranged to a matrix $\boldsymbol{D}_r \in \mathbb{C}^{M_s \times N}$, as shown in Fig.2. The grey rows represent to those pulses during which the radar detects airborne target (i.e., the orange pulses in Fig.1). We define a set Ψ to index the positions of those pulses employed for airborne target detection, which is given as:

$$\Psi = \bigcup_{i=1}^{L} \boldsymbol{\psi}_i, \quad \text{with} \quad \boldsymbol{\psi}_i = \{\delta_i, \delta_i + 1, \cdots, \delta_i + P - 1\}, \tag{7}$$

where δ_i denotes the location of the first pulse of the i-th airborne target detection.

Therefore, for a particular range bin, we denote the corresponding slow-time domain signal as $\boldsymbol{r} \in \mathbb{C}^{M_s \times 1}$, and the m-th element of $\boldsymbol{r}$ is given as:

$$\boldsymbol{r}[m] = \begin{cases} \boldsymbol{s}[m], & \text{if } m \notin \Psi \\ 0, & \text{if } m \in \Psi, \end{cases} \qquad m = 1, \cdots, M_s. \tag{8}$$

According to (8), $\boldsymbol{r}$ is an incomplete version of $\boldsymbol{s}$ (the slow-time domain signal obtained in conventional scheme, as shown in (2)). It is unreliable to use $\boldsymbol{r}$ to detect sea target. However, if we can recover the missing data in $\boldsymbol{r}$, the sea target detection can be accomplished with the performance equal or almost equal to that of the conventional scheme. In the next section, a Hankel structured low-rank matrix completion algorithm is elaborated to address this critical issue.

IV. HANKEL STRUCTURED LOW-RANK MATRIX COMPLETION

In this section, we will demonstrate how to recovery the missing data in $\boldsymbol{r}$. We first introduce the concept of Hankel matrix. Then, a recovery algorithm is introduced, the schematic diagram of which can refer to Fig.3. Finally, the convergence performance of the proposed algorithm is analyzed.

A. LOW-RANK MATRIX IN HANKEL STRUCTURE

Let us take the vector $\boldsymbol{s}$ in (2) as an example. The Hankel matrix of $\boldsymbol{s}$ with m_1 rows and m_2 columns is constructed as

$$\boldsymbol{S} = \begin{bmatrix} \boldsymbol{s}[1] & \boldsymbol{s}[2] & \cdots & \boldsymbol{s}[m_2] \\ \boldsymbol{s}[2] & \boldsymbol{s}[3] & \cdots & \boldsymbol{s}[m_2+1] \\ \vdots & \vdots & \ddots & \vdots \\ \boldsymbol{s}[m_1] & \boldsymbol{s}[m_1+1] & \cdots & \boldsymbol{s}[M] \end{bmatrix} \tag{9}$$

where $m_1 + m_2 - 1 = M_s$. In the following, we use $H(\cdot)$ to represent the operation that constructs a Hankel matrix with a vector. Similarly, for vector $\boldsymbol{r}$ in (8), we can obtain the corresponding Hankel matrix $\boldsymbol{R} = H(\boldsymbol{r})$.

As we have mentioned before, it is expected to obtain $\boldsymbol{s}$ by recovering $\boldsymbol{r}$. To achieve this, we resort to an equivalent scheme, i.e., obtaining $\boldsymbol{S}$ by recovering $\boldsymbol{R}$. For successful recovery, the following two requirements should be satisfied. (1) The matrix $\boldsymbol{S}$ is low rank. (2) The missing data in matrix $\boldsymbol{R}$ is sparse. As P (the number of pulses employed for airborne target detection) is much smaller than M_s, requirement (2) is easily satisfied. In the following, we prove that the requirement (1) is also meet. First, an important property of Hankel matrix is given in Lemma 1 [18].

Lemma 1: Given that the vector $\boldsymbol{s}$ is composed of d sinusoids and $d \ll \min(m_1, m_2)$, its Hankel matrix $\boldsymbol{S}$ has rank d if the sinusoidal frequencies are constant or the rank of $\boldsymbol{S}$ is close to d if the frequencies of sinusoids change significantly slow over the period of m_2.

According to (2), (4) and (6), the dominant components of $\boldsymbol{s}$ is 2 or 3 sinusoids, and the frequencies of them can be considered as time-varying slowly. Therefore, we can infer from Lemma 1 that the rank of $\boldsymbol{S}$ is close to 2 or 3. Moreover, as the number of pulses $M_s \gg 3$, the matrix $\boldsymbol{S}$ is low-rank.

As a conclusion, it is possible to successfully obtain $\boldsymbol{S}$ by recovering $\boldsymbol{R}$. And the method will be introduced in the following.

B. MATRIX RECOVERY METHOD

We first define an indicator $\boldsymbol{\phi} \in \mathbb{C}^{M_s \times 1}$ for $\boldsymbol{r}$, which is:

$$\boldsymbol{\phi}[m] = \begin{cases} 1 & \text{if } \boldsymbol{r}[m] \neq 0, \\ 0 & \text{if } \boldsymbol{r}[m] = 0. \end{cases} \tag{10}$$

Apparently, the value of $\boldsymbol{\phi}[m]$ indicates whether data exists in $\boldsymbol{r}[m]$. And accordingly, we calculate $\boldsymbol{\Phi} = H(\boldsymbol{\phi})$.

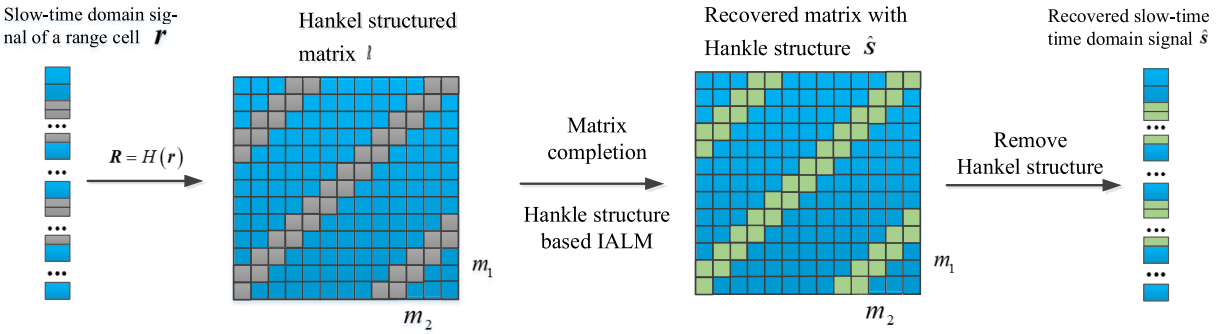

FIGURE 3. Schematic diagram of signal recovery. *To perform sea target target detection in a range bin, the corresponding slow-time domain signal r is first obtained after pulse compression, in which the data of some pulses is vacant. Then, a Hankel matrix $R = H(r)$ is developed. Next, Algorithm 1 is used to recover the missing data in R, thereby a Hankel matrix $\hat{S}$ is obtained. Finally, a vector $\hat{s}$ can be extracted from S.*

Then, the relationship between $\boldsymbol{S}$ and $\boldsymbol{R}$ can be expressed as follows:

$$\zeta_{\boldsymbol{\Phi}}(\boldsymbol{S}) = \boldsymbol{R} \quad \Leftrightarrow \quad \begin{cases} \boldsymbol{S} + \boldsymbol{E} = \boldsymbol{R} \\ \zeta_{\boldsymbol{\Phi}}(\boldsymbol{E}) = \boldsymbol{0}_{m_1 \times m_2}. \end{cases} \tag{11}$$

In (11), $\boldsymbol{E}$ is an error matrix. $\zeta_{\boldsymbol{\Phi}}(\cdot)$ is performed as follows:

$$[\zeta_{\boldsymbol{\Phi}}(\boldsymbol{S})]_{i,j} = \begin{cases} [\boldsymbol{S}]_{i,j}, & \text{if} \quad [\boldsymbol{\Phi}]_{i,j} = 1, \\ 0, & \text{if} \quad [\boldsymbol{\Phi}]_{i,j} = 0. \end{cases} \tag{12}$$

where $[\cdot]_{i,j}$ represents the (i, j)-th element of the corresponding matrix. More intuitively, $\zeta_{\boldsymbol{\Phi}}(\boldsymbol{E}) = \boldsymbol{0}_{m_1 \times m_2}$ means that the existing entries in $\boldsymbol{R}$ maintain the same as the corresponding entries in $\boldsymbol{S}$.

To obtain $\boldsymbol{S}$ by recovering $\boldsymbol{R}$, the typical optimization problem formulated with matrix completion theories [13], [17] is given as:

$$\begin{aligned} &\min_{\boldsymbol{S}} \|\boldsymbol{S}\|_*, \\ &\text{subject to } \zeta_{\boldsymbol{\Phi}}(\boldsymbol{S}) = \boldsymbol{R}. \end{aligned} \tag{13}$$

However in this work, the solution of (13) is further required to be a Hankel matrix so that a vector can be extracted from it. Therefore, (13) is improved to involve a Hankel structure constraint, resulting in the following optimization problem:

$$\begin{aligned} &\min_{\boldsymbol{S},\boldsymbol{E},\boldsymbol{\lambda}} \|\boldsymbol{S}\|_*, \\ &\text{subject to } \boldsymbol{S} + \boldsymbol{E} = \boldsymbol{R}, \quad \zeta_{\boldsymbol{\Phi}}(\boldsymbol{E}) = \boldsymbol{0}_{m_1 \times m_2}, \\ &\qquad \boldsymbol{S} = \sum_{m=1}^{M_s} \lambda_m \boldsymbol{B}_m, . \end{aligned} \tag{14}$$

where $\boldsymbol{\lambda} = [\lambda_1, \cdots, \lambda_m]^T$, with λ_m being the complex weight coefficient, and $\boldsymbol{B}_m$ is a $m_1 \times m_2$ basis matrix with the m-th anti-diagonal element equal to 1 and the others are 0.

To solve the problem in (14), we extend the inexact Augmented Lagrange Multiplier method (IALM) [19] and present a Hankel structure based IALM, which admits closed form updates and guarantees the Hankel constraint. The augmented Lagrange function of (14) is

$$\begin{aligned} &L(\boldsymbol{S}, \boldsymbol{E}, \boldsymbol{\lambda}, \boldsymbol{Y}_1, \boldsymbol{Y}_2, \mu) \\ &= \|\boldsymbol{S}\|_* + \langle \boldsymbol{Y}_1, \boldsymbol{R} - \boldsymbol{S} - \boldsymbol{E} \rangle \\ &\quad + \frac{\mu}{2} \|\boldsymbol{R} - \boldsymbol{S} - \boldsymbol{E}\|_F^2 + \left\langle \boldsymbol{Y}_2, \sum_{m=1}^{M_s} \lambda_m \boldsymbol{B}_m - \boldsymbol{S} \right\rangle \\ &\quad + \frac{\mu}{2} \left\| \sum_{m=1}^{M_s} \lambda_m \boldsymbol{B}_m - \boldsymbol{S} \right\|_F^2, \end{aligned} \tag{15}$$

where $\boldsymbol{Y}_1, \boldsymbol{Y}_2 \in \mathbb{C}^{m_1 \times m_2}$ are Lagrange multiplier matrices. μ is a penalty parameter. Based on (15), the iteration is processed as follows

$$\boldsymbol{S}^{(k+1)} = \arg\min_{\boldsymbol{S}} L(\boldsymbol{S}, \boldsymbol{\lambda}^{(k)}, \boldsymbol{E}^{(k)}, \boldsymbol{Y}_1^{(k)}, \boldsymbol{Y}_2^{(k)}, \mu^{(k)}) \tag{16a}$$

$$\boldsymbol{\lambda}^{(k+1)} = \arg\min_{\boldsymbol{\lambda}} L(\boldsymbol{S}^{(k+1)}, \boldsymbol{\lambda}, \boldsymbol{E}^{(k)}, \boldsymbol{Y}_1^{(k)}, \boldsymbol{Y}_2^{(k)}, \mu^{(k)}) \tag{16b}$$

$$\boldsymbol{E}^{(k+1)} = \arg\min_{\zeta_{\boldsymbol{\Phi}}(\boldsymbol{E})=\boldsymbol{0}} L(\boldsymbol{S}^{(k+1)}, \boldsymbol{\lambda}^{(k+1)}, \boldsymbol{E}, \boldsymbol{Y}_1^{(k)}, \boldsymbol{Y}_2^{(k)}, \mu^{(k)}) \tag{16c}$$

$$\boldsymbol{Y}_1^{(k+1)} = \boldsymbol{Y}_1^{(k)} + \mu^{(k)}(\boldsymbol{R} - \boldsymbol{S}^{(k+1)} - \boldsymbol{E}^{(k+1)}) \tag{16d}$$

$$\boldsymbol{Y}_2^{(k+1)} = \boldsymbol{Y}_2^{(k)} + \mu^{(k)}(\sum_{m=1}^{M_s} \lambda_m^{(k+1)} \boldsymbol{B}_m - \boldsymbol{S}^{(k+1)}) \tag{16e}$$

$$\mu^{(k+1)} = \rho \mu^{(k)} \tag{16f}$$

where $\rho > 1$ and k is the index of iteration.

Equations (16d), (16e) and (16f) respectively give the closed-form solutions for updating $\boldsymbol{Y}_1^{(k+1)}$, $\boldsymbol{Y}_2^{(k+1)}$ and $\mu^{(k+1)}$. In the following, we will show that the other variables also have closed-form solutions for updating.

1) UPDATE S

Problem (16a) can be recast to the following unconstrained optimization problem:

$$\min_{\boldsymbol{S}} \|\boldsymbol{S}\|_* + \mu^{(k)} \left\| \boldsymbol{S} - \boldsymbol{Q}^{(k)} \right\|_F^2 \tag{17}$$

where $\boldsymbol{Q}^{(k)} = \frac{1}{2}[\boldsymbol{R} - \boldsymbol{E}^{(k)} + \sum_{m=1}^{M_s} \lambda_m^{(k)} \boldsymbol{B}_m + \mu^{(k)-1}(\boldsymbol{Y}_1^{(k)} + \boldsymbol{Y}_2^{(k)})]$. According to the Theorem 2.1 in [14], problem (17) has a

closed-form solution:

$$\boldsymbol{S}^{(k+1)} = \boldsymbol{U}Shrink_{\frac{1}{2\mu^{(k)}}}(\boldsymbol{\Sigma})\boldsymbol{V}^T \tag{18}$$

where $(\boldsymbol{U}, \boldsymbol{\Sigma}, \boldsymbol{V}) = \text{svd}(\boldsymbol{Q}^{(k)})$ and $Shrink_{\varepsilon}(\cdot)$ is an element-wise soft-thresholding operator:

$$Shrink_{\varepsilon}(x) = \begin{cases} 0, & \text{if } |x| \le \varepsilon \\ x - \varepsilon, & \text{if } x > \varepsilon \\ x + \varepsilon, & \text{if } x < -\varepsilon \end{cases} \tag{19}$$

with x being a real value and $\varepsilon > 0$.

2) UPDATE λ

The optimization problem (16b) for updating $\boldsymbol{\lambda}$ can be expressed as follows:

$$\min_{\boldsymbol{\lambda}} \left\| \sum_{m=1}^{M_s} \lambda_m \boldsymbol{B}_m - \boldsymbol{S}^{(k+1)} + (\boldsymbol{Y}_2^{(k)}/\mu^{(k)}) \right\|_F^2. \tag{20}$$

Defining $\boldsymbol{F}^{(k)} = \sum_{m=1}^{M_s} \lambda_m^{(k)} \boldsymbol{B}_m - \boldsymbol{S}^{(k+1)} + (\boldsymbol{Y}_2^{(k)}/\mu^{(k)})$, we have

$$\frac{\partial \left\| \boldsymbol{F}^{(k)} \right\|_F^2}{\partial \lambda_m^{(k)}} = 2\lambda_m^{(k)*} \left\| \boldsymbol{B}_m \right\|_F^2 - 2\text{tr}\{\boldsymbol{B}_m^T(\boldsymbol{S}^{(k+1)} - \boldsymbol{Y}_2^{(k)}/\mu^{(k)})\},$$

and therefore

$$\frac{\partial \left\| \boldsymbol{F}^{(k)} \right\|_F^2}{\partial \lambda_m^{(k)} \partial \lambda_m^{(k)*}} = 2 \left\| \boldsymbol{B}_m \right\|_F^2 > 0. \tag{21}$$

Equation (21) indicates that problem (20) is quadratic and convex with respect to $\boldsymbol{\lambda}$. Therefore, we can update each element of $\boldsymbol{\lambda}^{(k)}$ by letting $\partial \left\| \boldsymbol{F}^{(k)} \right\|_F^2 / \partial \lambda_m^{(k)} = 0$, resulting:

$$\lambda_m^{(k+1)} = \frac{1}{\left\| \boldsymbol{B}_m \right\|_F^2} \text{tr}\left\{ \boldsymbol{B}_m^T(\boldsymbol{S}^{(k+1)} - \boldsymbol{Y}_2^{(k)}/\mu^{(k)}) \right\}, \quad m = 1, \cdots M. \tag{22}$$

3) UPDATE *E*

According to (16c), we have

$$\min_{\boldsymbol{E}} \left\| \boldsymbol{R} - \boldsymbol{S}^{(k+1)} - \boldsymbol{E} + \boldsymbol{Y}_1^{(k)}/\mu^{(k)} \right\|_F^2 \quad \text{subject to } \zeta_{\boldsymbol{\Phi}}(\boldsymbol{E}) = \boldsymbol{0}_{m_1 \times m_2}. \tag{23}$$

For problem (23), there is a closed-form solution, given as

$$\boldsymbol{E}^{(k+1)} = \zeta_{\bar{\boldsymbol{\Phi}}}(\boldsymbol{R} - \boldsymbol{S}^{(k+1)} + \boldsymbol{Y}_1^{(k)}/\mu^{(k)}), \tag{24}$$

where

$$[\bar{\boldsymbol{\Phi}}]_{i,j} = \begin{cases} 1, & \text{if } [\boldsymbol{\Phi}]_{i,j} = 0, \\ 0, & \text{if } [\boldsymbol{\Phi}]_{i,j} = 1. \end{cases} \tag{25}$$

Finally, the entire algorithm for recovering the incomplete slow-time domain signal $\boldsymbol{r}$ is described in Algorithm 1.

Algorithm 1 Recovering $\boldsymbol{r}$ via Hankel Structure Based IALM

Input: Incomplete slow-time domain signal $\boldsymbol{r}$ and $\boldsymbol{R} = H(\boldsymbol{r})$.
Initial value: $\boldsymbol{S}^{(0)} = \boldsymbol{Y}_1^{(0)} = \boldsymbol{Y}_2^{(0)} = \boldsymbol{0}_{m_1 \times m_2}$; $\boldsymbol{\lambda}^{(0)} = \boldsymbol{0}_{M_s \times 1}$; $\rho = 1.4$; $\mu^{(0)} = 1/2\|\boldsymbol{R}\|_F$; $k = 0$.

1: **while** not converged **do**
2: $(\boldsymbol{U}, \boldsymbol{\Sigma}, \boldsymbol{V}) = \text{svd}\left(\boldsymbol{Q}^{(k)}\right)$
3: $\boldsymbol{S}^{(k+1)} = \boldsymbol{U}Shrink_{\frac{1}{2\mu^{(k)}}}(\boldsymbol{\Sigma})\boldsymbol{V}^T$
4: $\lambda_m^{(k+1)} = \frac{1}{\|\boldsymbol{B}_m\|_F^2} \text{tr}\left\{ \boldsymbol{B}_m^T(\boldsymbol{S}^{(k+1)} - \boldsymbol{Y}_2^{(k)}/\mu^{(k)}) \right\}$
5: $\boldsymbol{E}^{(k+1)} = \zeta_{\bar{\boldsymbol{\Phi}}}(\boldsymbol{R} - \boldsymbol{S}^{(k+1)} + \boldsymbol{Y}_2^{(k)}/\mu^{(k)})$
6: $\boldsymbol{Y}_1^{(k+1)} = \boldsymbol{Y}_1^{(k)} + \mu^{(k)}(\boldsymbol{R} - \boldsymbol{S}^{(k+1)} - \boldsymbol{E}^{(k+1)})$
7: $\boldsymbol{Y}_2^{(k+1)} = \boldsymbol{Y}_2^{(k)} + \mu^{(k)}(\sum_{m=1}^{M_s} \lambda_m^{(k+1)} \boldsymbol{B}_m - \boldsymbol{S}^{(k+1)})$
8: $\mu^{(k+1)} = \rho\mu^{(k)}, \quad k = k + 1$
9: **end while**

Output: $\hat{\boldsymbol{s}} = [\lambda_1^{(k+1)}, \cdots, \lambda_{M_s}^{(k+1)}]^T$, which is the recovered slow-time domain signal.

C. CONVERGENCE PROPERTY

The convergence of standard ILAM for tackling the linearly constrained convex programming has been well studied in [19], [27], where the objective function is assumed to have two blocks. However, problem (14) involves a smooth objective function with three blocks ($\boldsymbol{S}$, $\boldsymbol{E}$ and $\boldsymbol{\lambda}$), therefore, the convergence of proposed Hankel structure based ILAM need a further discussion. According to the sufficient (may not necessary) condition in [28], the algorithm 1 is ensured to converge when the gap of each iteration is monotonically decreasing. That is to say, the error $\boldsymbol{\varepsilon}^{(k)}$ in Algorithm 1:

$$\boldsymbol{\varepsilon}^{(k)} = \left\| \boldsymbol{S}^{(k)} - \widehat{\boldsymbol{S}} \right\|_F + \left\| \boldsymbol{E}^{(k)} - \widehat{\boldsymbol{E}} \right\|_F + \left\| \boldsymbol{\lambda}^{(k)} - \widehat{\boldsymbol{\lambda}} \right\|_F \tag{26}$$

should be monotonically decreasing, where $(\widehat{\boldsymbol{S}}, \widehat{\boldsymbol{E}}, \widehat{\boldsymbol{\lambda}})$ is the optimal solution for minimizing the Lagrangian function in (15). As the convexity of the Lagrangian function could guarantee the monotonically decreasing to some extent [29], therefore Algorithm 1 could be well expected to have good convergence properties.

There, following with the discussion in [19], the stopping criteria of Algorithm 1 are given as follows:

$$\begin{aligned} \xi_1 &= \|\boldsymbol{R} - \boldsymbol{S}^{(k)} - \boldsymbol{E}^{(k)}\|_F / \|\boldsymbol{R}\|_F < \epsilon_1, \\ \xi_2 &= \mu^{(k-1)} \|\boldsymbol{E}^{(k)} - \boldsymbol{E}^{(k-1)}\|_F / \|\boldsymbol{R}\|_F < \epsilon_2, \\ \xi_3 &= \|\boldsymbol{S}^{(k)} - \sum_{m=1}^{M_s} \lambda_m^{(k)} \boldsymbol{B}_m\|_F / \|\boldsymbol{R}\|_F < \epsilon_3, \end{aligned} \tag{27}$$

where the thresholds ϵ_1 ϵ_2 and ϵ_3 should be sufficient small. With the above stopping criteria, the convergence and complexity of Algorithm 1 will be further evaluated through simulation experiment.

V. EXPERIMENTAL DATA PROCESSING RESULTS

In this section, a series of numerical simulations are conducted based on the experimental data from a sky-wave OTH

TABLE 2. Parameters of sky-wave OTH radar.

Targets	Pulse repetition interval (ms)	Number of pulses in a CIT	Coherent integration time (sec)	Bandwidth (kHz)
aircraft	$T_a = 12$	$M_a = 128$	$\text{CIT}^{(a)} = 1.536$	2
ship	$T_s = 100$	$M_s = 512$	$\text{CIT}^{(s)} = 51.2$	10

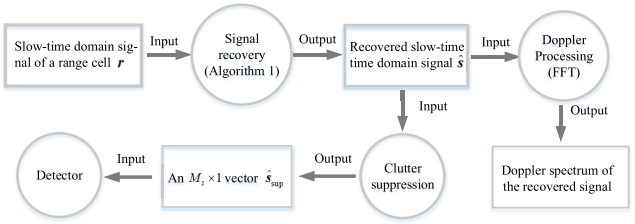

FIGURE 4. Operations performed on r.

radar, which transmits the LFM waveform. The carry frequency of the radar is $f_0 = 20$ MHz and the other parameters are listed in Table 2.

Notice that the coherent integration time actually required by the airborne target detection is 1.536sec, but we set $\text{CIT}^{(a)} = 2$sec. There, the additional 0.464 seconds is reserved for array to change the beamforming direction and the parameter settings. We totally insert three airborne target detections, which respectively start at the 100-th, 285-th, and 400-th pulses. Since the performance of airborne target detection is guaranteed, the key for evaluating the proposed scheme is sea target detection performance. The signal recovery results and signal processing results of sea surface echo are given and discussed in the following.

Generally, the sea surface echo successively undergoes carrier frequency removal, beamforming, pulse compression (matched filtering) and phase compensation, after which the slow time-domain signal of each range bin (i.e., $\boldsymbol{r}$ in (8)) is obtained. In each $\boldsymbol{r}$, there are 60 elements vacant. Then, for the purpose of target detection, $\boldsymbol{r}$ will further undergo a series of signal processing.

As shown in Fig.4, $\boldsymbol{r}$ is firstly recovered by the proposed Algorithm 1, obtaining a recovered slow-time domain signal $\hat{\boldsymbol{s}}$. Next, $\hat{\boldsymbol{s}}$ is processed by a clutter filter, with an $M_s \times 1$ vector generated as the indicator for detector [20, Section 4.2.3.1]. Besides, for a certain range bin, we can obtain the Doppler spectrum of echo signal by performing fast Fourier transform (FFT) on the corresponding slow-time domain signal [20, Section 4.2.3.2]. The Doppler spectrum can reflect the power of signal components with different Doppler frequencies.

In the following experiments, we focus on the 510-th range bin in which a sea target with Doppler frequency $f_d = 1.445$Hz exists. The slow-time domain signals appearing behind are both corresponding to the 510-th range bin. The signal processing results of $\hat{\boldsymbol{s}}$ are fully analyzed, with the results of $\boldsymbol{r}$ and $\boldsymbol{s}$ also given as references.

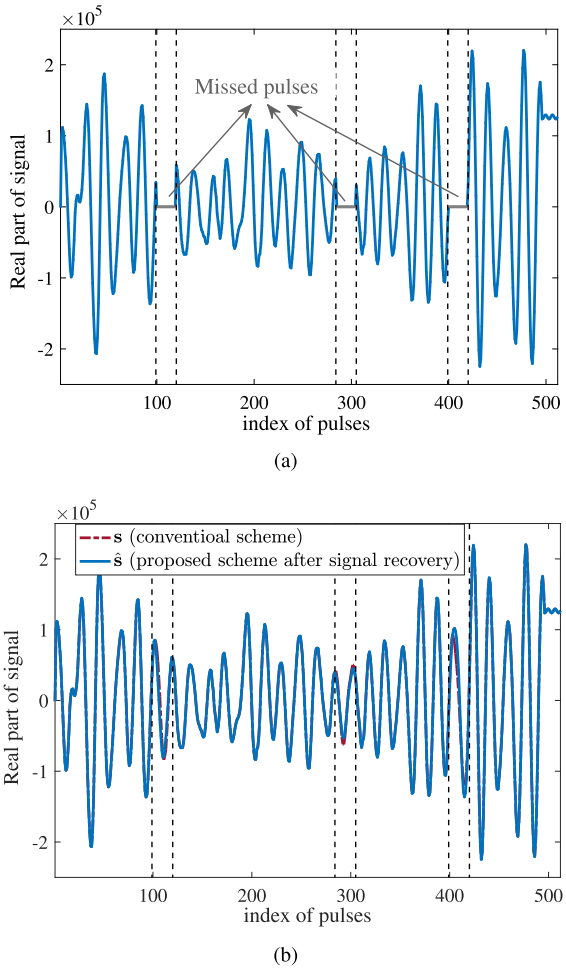

FIGURE 5. Real parts of the slow-time domain signals: (a) r-obtained with proposed scheme (b) $\hat{s}$-obtained with proposed scheme after signal recovery and s-obtained with conventional scheme.

A. SIGNAL RECOVERY RESULT

First, we depict in Fig.5 the real parts of $\boldsymbol{s}$, $\boldsymbol{r}$ and $\hat{\boldsymbol{s}}$. More specifically, Fig.5(a) shows the real part of $\boldsymbol{r}$. In $\boldsymbol{r}$, the elements corresponding to some pulses are zero, since the radar can not receive echo from sea surface during these pulses. In Fig.5(b), the real parts of $\boldsymbol{s}$ and $\hat{\boldsymbol{s}}$ are depicted. It can be seen that the vacant elements in $\boldsymbol{r}$ are restored in $\hat{\boldsymbol{s}}$, and the recovered signal $\hat{\boldsymbol{s}}$ is highly similar to $\boldsymbol{s}$, indicating that the effectiveness of Algorithm 1 on recovering the incomplete signal $\boldsymbol{r}$. (The imaginary parts of $\boldsymbol{s}$, $\boldsymbol{r}$ and $\hat{\boldsymbol{s}}$ shows similar results and therefore are not displayed to avoid redundancy.)

Next, we evaluate the signal recovery performance through Doppler spectrum. The Doppler spectrum of the echo signal in a range bin is obtained by performing FFT on the corresponding slow-time domain signal, which can reflect the power of signal components with different Doppler frequencies.

In Fig.6, totally three Doppler spectra (after normalization) are depicted, which are respectively associated with $\boldsymbol{s}$, $\boldsymbol{r}$ and $\hat{\boldsymbol{s}}$. Moreover, the horizontal axis corresponds to the Doppler frequency of the signal component, which is from

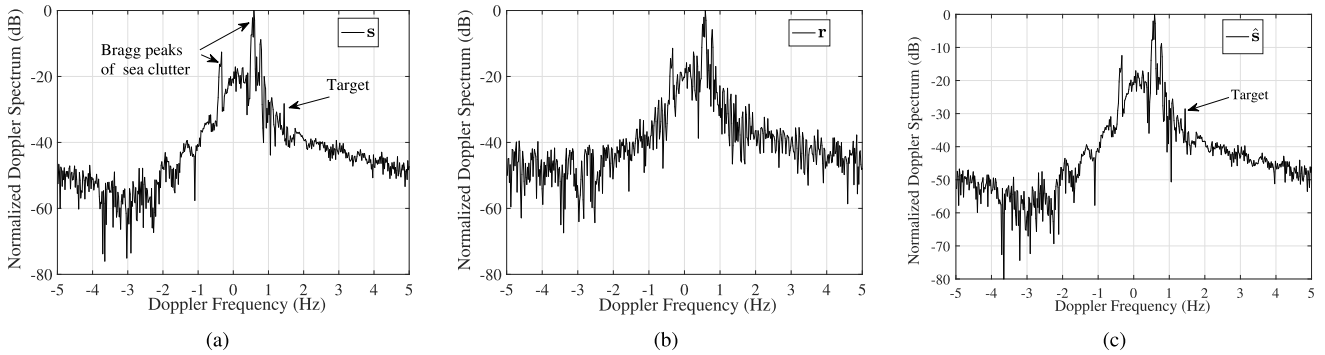

FIGURE 6. Normalized Doppler spectrum of signal in 510-th range bin (where a sea target exists): (a) the conventional scheme, (b) the proposed scheme before signal recovery and (c) the proposed scheme after signal recovery.

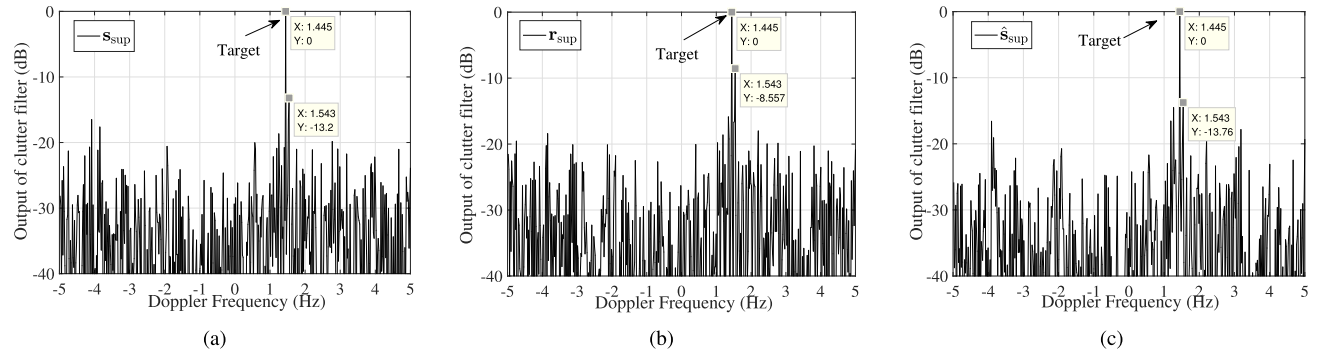

FIGURE 7. Results of clutter suppression: (a) the conventional scheme, (b) the proposed scheme before signal recovery and (c) the proposed scheme after signal recovery.

$-\frac{1}{2T_s}$ to $\frac{1}{2T_s}$, and the ordinate axis denotes the power of the corresponding signal component. From Fig.6(a) and Fig.6(b), we can observe that the Doppler spectrum of $\boldsymbol{r}$ is severely damaged, in which the target is totally submerged in the sea clutter. This is because that the $\boldsymbol{r}$ is obtained with the incomplete sea surface echo, in which the power of target is not sufficiently accumulated. On the other hand, Fig.6(c) shows a Doppler spectrum similar to that in Fig.6(a). Importantly, a spike re-appears at the Doppler frequency of the sea target. This result means that the proposed algorithm guarantees the coherence of signal when recovering $\boldsymbol{r}$.

B. TARGET DETECTION PERFORMANCE

Through the above two experiments, we intuitively show the signal recovery result from time domain and frequency domain. Beside, the Doppler spectra given in Fig.6 reflect that the sea clutter is very strong in the echo which seriously affects the sea target detection. In order to evaluate the sea target detection performance, it is necessary to concern the result after sea clutter suppression. Therefore, the signal $\hat{\boldsymbol{s}}$ is supposed to be processed by a clutter filter [30], [31], through which an $M_s \times 1$ vector $\hat{\boldsymbol{s}}_{\text{sup}}$ can be obtained to reflect the power of each signal component after clutter suppression. Following with [20, Equations (4.102)-(4.103)], the m-th element of $\hat{\boldsymbol{s}}_{\text{sup}}$ is calculated as

$$\hat{\boldsymbol{s}}_{\text{sup}}[m] = \left[\boldsymbol{R}_{\boldsymbol{c}}^{-1}\boldsymbol{\alpha}(f_{dm})\right]^H \hat{\boldsymbol{s}}, \tag{28}$$

where $\boldsymbol{R}_{\boldsymbol{c}} \in \mathbb{C}^{M_s \times M_s}$ is the covariance matrix of the clutter signal $\boldsymbol{c}$, and

$$\boldsymbol{\alpha}(f_{dm}) = [1,\ e^{j2\pi f_{dm}}, \ldots, e^{j2\pi(M_s-1)f_{dm}}]^T$$

is the steering vector corresponding to the Doppler frequency f_{dm}. We denote that $\hat{\boldsymbol{s}}_{\text{sup}}[m]$ is a statistic for detection. That is to say, if $\hat{\boldsymbol{s}}_{\text{sup}}[m]$ is higher than a set threshold, the detector considers that a target with Doppler frequency f_{dm} exists.

In Fig.7(c), we depict $\hat{\boldsymbol{s}}_{\text{sup}}$, while $\boldsymbol{s}_{\text{sup}}$ and $\boldsymbol{r}_{\text{sup}}$ are given in Fig.7(a) and Fig.7(b). Both of them are normalized. It can be seen that, after clutter suppression, the power of target component ($f_d = 1.455$Hz) is significantly higher than those of the other signal components. Therefore, with an appropriate threshold, the detector can correctly determine that there is a target with Doppler frequency 1.455Hz exists, and the signal component with other Doppler frequencies does not cause misjudgment.

Based on the above discussion, the key factors that affect the target detection performance are the main-to-side lobe ratio (MSLR) and peak-to-average ratio (PAR) of clutter filter output. Using $\hat{\boldsymbol{s}}_{\text{sup}}$ as an example, its MSLR and PAR are

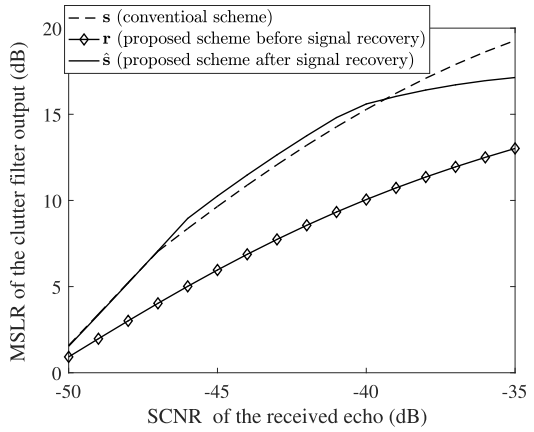

FIGURE 8. The main-to-side lobe ratio (MSLR) versus the SCNR of the received echo.

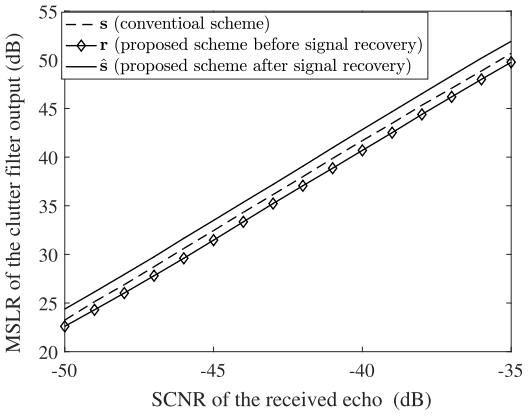

FIGURE 9. The peak-to-average ratio (PAR) versus the SCNR of the received echo.

respectively calculated as

$$\mathrm{MSLR} = 20\log\frac{\hat{\boldsymbol{s}}_{\mathrm{sup}}[m_0]}{\max\{\hat{\boldsymbol{s}}_{\mathrm{sup}}[m]\,|m=1,\ldots,M_s,\, m\neq m_0\}}$$

and

$$\mathrm{PAR} = 20\log\frac{\hat{\boldsymbol{s}}_{\mathrm{sup}}\,[m_0]}{\mathrm{sum}\left\{\hat{\boldsymbol{s}}_{\mathrm{sup}}\right\}},$$

where $\hat{\boldsymbol{s}}_{\mathrm{sup}}\,[m_0]$ denote the maximum element in $\hat{\boldsymbol{s}}_{\mathrm{sup}}$.

We denote that larger MSLR or PAR results in lower false alarm probability and vice versa. According to Fig.7, the MSLRs of $\boldsymbol{s}_{\mathrm{sup}}$ and $\hat{\boldsymbol{s}}_{\mathrm{sup}}$ are close (13.2dB and 13.76dB, respectively), while that of $\boldsymbol{r}_{\mathrm{sup}}$ is significantly smaller (about 8.56dB). This indicates that the recovered signal can achieve a target detection performance similar to that achieved by the conventional scheme.

Up to now, we follow with the signal processing flew given in Fig.4, comparing the performance of the proposed scheme and conventional scheme step by step. Also, we illustrate that the PAR and MSLR of clutter filter output are the two key indicators to assess the sea target detection performance. In the following, a more comprehensive evaluation to the sea target detection performance is conducted based on these two indicators. We change the power of the target to make the signal to clutter plus noise ratios (SCNR) of received sea surface echo different. Then for different SCNR levels, we obtain $\boldsymbol{s}_{\mathrm{sup}}$, $\boldsymbol{r}_{\mathrm{sup}}$ and $\hat{\boldsymbol{s}}_{\mathrm{sup}}$ and calculate the corresponding PARs and MSLRs. The results are concluded in Fig.8 and Fig.9.

First, we can observe that the PAR and MSLR obtained by $\hat{\boldsymbol{s}}$ are larger than those obtained by $\boldsymbol{r}$, regardless of SCNR level in echo signal. This shows that the sea target detection performance can be improved in different SCNRs cases, indicating the reliability of the proposed algorithm. Moreover, by observing the results of $\hat{\boldsymbol{s}}$ and $\boldsymbol{s}$, we have the following statements.

(1) When the SCNR of echo signal is small, the PAR and MSLR obtained by $\hat{\boldsymbol{s}}$ are slightly higher than those obtained by $\boldsymbol{s}$, which indicates that $\hat{\boldsymbol{s}}$ can achieve a better sea target detection performance than $\hat{\boldsymbol{s}}$ in this case. This is because that the Algorithm 1 preferentially recovers the principal components (i.e., target and clutter), and the noise component is not well recovered. As a consequence, the power of the sea target component in $\hat{\boldsymbol{s}}$ is close to that in $\boldsymbol{s}$, while the power of the noise component is smaller than that in $\boldsymbol{s}$. Therefore, in the case that SCNR is small (which means that the noise power is relatively strong in $\boldsymbol{s}$), the proposed scheme can provide a better target detection performance.

(2) When the SCNR is large, the MSLR of $\hat{\boldsymbol{s}}$ is slightly worse than that of $\boldsymbol{s}$. In the case of large SCNR, the decisive factor of MSLR is the power of signal component and the effect of noise is relatively weak. Considering that the recovery algorithm can not fully recovery the sea target to bring it to the same level as in $\boldsymbol{s}$, such result is reasonable.

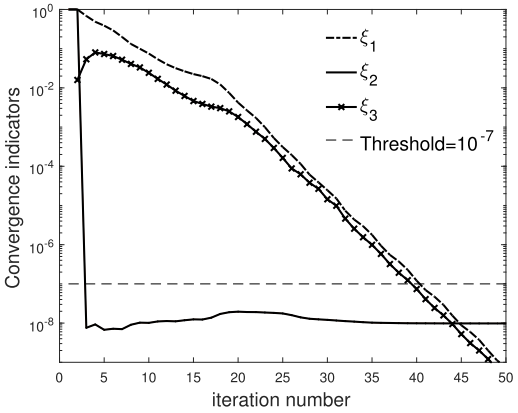

FIGURE 10. Convergence indicators at each iteration.

C. CONVERGENCE PERFORMANCE OF ALGORITHM 1

Finally, we verify the convergence of proposed Algorithm 1. Reviewing the stopping criteria given in (27), Fig.10 exhibits the iteration curves of ξ_1, ξ_2 and ξ_3.

With the convergence threshold setting as $\epsilon_1 = \epsilon_2 = \epsilon_3 = 10^{-7}$, condition ξ_2 can meet the convergence requirement quickly. Bedsides, conditions ξ_1 and ξ_3 decrease at approximately exponential speed. After 41 iterations, all the three conditions reach the threshold. The results show that

the convergence speed of the proposed algorithm is relatively fast, and therefore it does not consume a large amount of calculation.

VI. CONCLUSION

In this paper, we propose a new timeframe multiplexed scheme for OTH radar detecting sea target and airborne targets in different directions. The scheme inserts several airborne target detections into a CIT of sea target. Compared with the conventional scheme, the frequency of airborne target detection is improved, which facilitates tracking and monitoring of airborne target. Besides, a signal recovery algorithm is proposed to recover incomplete signal received from sea surface, so as to keep the detection performance of sea target the same or close to the conventional scheme. Experimental examples show the signal recovery result, proving the effectiveness of the proposed algorithm. Besides, the sea target detection performance of the proposed scheme is compared with the conventional scheme. The results verify that the proposed scheme can improve the detection frequency of airborne target without losing the detection performance of the sea target.

ACKNOWLEDGMENT

The authors would like to thank Dr. Xianxiang Yu from UESTC for discussions on this topic.

REFERENCES

[1] J. M. Headrick and S. J. Anderson, "HF over-the-horizon radar," in *Radar Handbook*. New York, NY, USA: McGraw-Hill, 2008, pp. 1–83.

[2] T. Thayaparan, D. Dupont, Y. Ibrahim, and R. Riddolls, "High-frequency ionospheric monitoring system for Over-the-Horizon radar in canada," *IEEE Trans. Geosci. Remote Sens.*, vol. 57, no. 9, pp. 6372–6384, Sep. 2019.

[3] R. J. Riddolls, "High-latitude application of three-dimensional over-the-horizon radar," *IEEE Aerosp. Electron. Syst. Mag.*, vol. 32, no. 12, pp. 36–43, Dec. 2017.

[4] M. Nosrati, S. Shahsavari, S. Lee, H. Wang, and N. Tavassolian, "A concurrent dual-beam phased-array Doppler radar using MIMO beamforming techniques for short-range vital-signs monitoring," *IEEE Trans. Antennas Propag.*, vol. 67, no. 4, pp. 2390–2404, Apr. 2019.

[5] X. Chen, T. Shu, K.-B. Yu, J. He, and W. Yu, "Joint adaptive beamforming techniques for distributed array radars in multiple mainlobe and sidelobe jammings," *IEEE Antennas Wireless Propag. Lett.*, vol. 19, no. 2, pp. 248–252, Feb. 2020.

[6] J. Barnum, "Ship detection with high-resolution HF skywave radar," *IEEE J. Ocean. Eng.*, vol. 11, no. 2, pp. 196–209, Apr. 1986.

[7] L. Ya-jun, X. Rong-qing, S. Chao, and W. Yin-sheng, "Simulation analysis and experimentation study on sea clutter spectrum for high-frequency hybrid sky-surface wave propagation mode," *IET Radar, Sonar Navigat.*, vol. 8, no. 8, pp. 917–930, Oct. 2014.

[8] S. Anderson, "OTH radar phenomenology: Signal interpretation and target characterization at HF," *IEEE Aerosp. Electron. Syst. Mag.*, vol. 32, no. 12, pp. 4–16, Dec. 2017.

[9] J. A. Olkin, W. C. Nowlin, and J. R. Barnum, "Detection of ships using OTH radar with short integration times," in *Proc. IEEE Nat. Radar Conf.*, May 1997, pp. 1–6.

[10] S. J. Anderson, A. R. Mahoney, and M. D. E. Turley, "Applications of super resolution techniques to HF Radar sea echo analysis," in *Proc. Pacific Ocean Remote Sens. Conf.*, Melbourne, VIC, Australia, 1994, pp. 491–499.

[11] X. Guo, J.-L. Ni, and G.-S. Liu, "Ship detection with short coherent integration time in over-the-horizon radar," in *Proc. Int. Conf. Radar*, 2003, pp. 667–671.

[12] S. Shang and Z. Ning, "Low speed target detection with short cit in HF surface wave radar," in *Proc. 2nd Int. Conf. Signal Process. Syst.*, vol. 2, Jul. 2010, p. V2-499.

[13] M. A. Davenport and J. Romberg, "An overview of low-rank matrix recovery from incomplete observations," *IEEE J. Sel. Topics Signal Process.*, vol. 10, no. 4, pp. 608–622, Jun. 2016.

[14] J.-F. Cai, E. J. Candés, and Z. Shen, "A singular value thresholding algorithm for matrix completion," *SIAM J. Optim.*, vol. 20, no. 4, pp. 1956–1982, Jan. 2010.

[15] Y. Chen and Y. Chi, "Spectral compressed sensing via structured matrix completion," 2013, *arXiv:1304.4610*. [Online]. Available: https://arxiv.org/abs/1304.4610

[16] T. Zhou and D. Tao, "GoDec: Randomized low-rank and sparse matrix decomposition in noisy case," in *Proc. Int. Conf. Mach. Learn. (ICML)*, Jun. 2011, pp. 33–40.

[17] E. J. Candès and B. Recht, "Exact matrix completion via convex optimization," *Found. Comput. Math.*, vol. 9, no. 6, p. 717, 2009.

[18] M. W. Y. Poon, R. H. Khan, and S. Le-Ngoc, "A singular value decomposition (SVD) based method for suppressing ocean clutter in high frequency radar," *IEEE Trans. Signal Process.*, vol. 41, no. 3, pp. 1421–1425, Mar. 1993.

[19] Z. Lin, M. Chen, and Y. Ma, "The augmented Lagrange multiplier method for exact recovery of corrupted low-rank matrices," *J. Struct. Biol.*, vol. 181, no. 2, pp. 116–127, Sep. 2010.

[20] G. A. Fabrizio, *High Frequency Over-the-Horizon Radar: Fundamental Principles, Signal Processing, and Practical Applications*. New York, NY, USA: McGraw-Hill, 2013.

[21] G. Wang, X.-G. Xia, B. T. Root, V. C. Chen, Y. Zhang, and M. Amin, "Manoeuvring target detection in over-the-horizon radar using adaptive clutter rejection and adaptive chirplet transform," *IEE Proc. Radar, Sonar Navigat.*, vol. 150, no. 4, pp. 292–298, 2003.

[22] A. Yasotharan and T. Thayaparan, "Time-frequency method for detecting an accelerating target in sea clutter," *IEEE Trans. Aerosp. Electron. Syst.*, vol. 42, no. 4, pp. 1289–1310, Oct. 2006.

[23] Y. Li, T. Wang, B. Liu, L. Yang, and G. Bi, "Ground moving target imaging and motion parameter estimation with airborne dual-channel CSSAR," *IEEE Trans. Geosci. Remote Sens.*, vol. 55, no. 9, pp. 5242–5253, Sep. 2017.

[24] R. H. Khan, "Ocean-clutter model for high-frequency radar," *IEEE J. Ocean. Eng.*, vol. 16, no. 2, pp. 181–188, Apr. 1991.

[25] S. Anderson, "Multiple scattering of HF surface waves: Implications for radar design and sea clutter interpretation," *IET Radar, Sonar Navigat.*, vol. 4, no. 2, pp. 195–208, 2010.

[26] J. Hu, C. Jian, C. Zhuo, H. Li, and J. Xie, "Knowledge-aided ocean clutter suppression method for sky-wave Over-the-Horizon radar," *IEEE Geosci. Remote Sens. Lett.*, vol. 15, no. 3, pp. 355–358, Mar. 2018.

[27] Y. Zhang, "Recent advances in alternating direction methods: Practice and theory," presented at the IPAM Workshop Continuous Optim.

[28] G. Liu, Z. Lin, S. Yan, J. Sun, Y. Yu, and Y. Ma, "Robust recovery of subspace structures by low-rank representation," *IEEE Trans. Pattern Anal. Mach. Intell.*, vol. 35, no. 1, pp. 171–184, Jan. 2013.

[29] J. Eckstein and D. P. Bertsekas, "On the douglas—Rachford splitting method and the proximal point algorithm for maximal monotone operators," *Math. Program.*, vol. 55, nos. 1–3, pp. 293–318, 1992.

[30] W. L. Melvin, "Space-time adaptive radar performance in heterogeneous clutter," *IEEE Trans. Aerosp. Electron. Syst.*, vol. 36, no. 2, pp. 621–633, Apr. 2000.

[31] Z. Ji, C. Yi, J. Xie, and Y. Li, "The application of JDL to suppress sea clutter for shipborne HFSWR," *Int. J. Antennas Propag.*, vol. 2015, pp. 1–6, Apr. 2015.

ZHAOYI WANG was born in Xuzhou, China, in 1992. He received the B.S. degrees in electronic information engineering and finance from the University of Electronic Science and Technology of China (UESTC), Chengdu, China, in 2014. He is currently pursuing the Ph.D. degree with the School of Information and Communication Engineering, UESTC, China.

His research interests include radar signal processing, clutter modeling and suppression in OTH radar, and interference cancellation in OTH radar.

SHENGNAN SHI received the B.S. degree in communication engineering from the University of Harbin Engineering University (HEU), Harbin, China, in 2016. She is currently pursuing the Ph.D. degree in signal and information processing with the University of Electronic Science and Technology of China (UESTC), Chengdu, China.

Her research interests include radar waveform design, adaptive signal processing, and optimization theory.

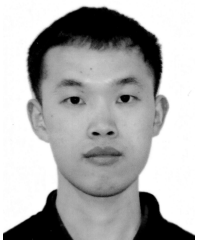

ZIYANG CHENG was born in Yingcheng, Hubei, China, in 1990. He received the M.S. and Ph.D. degrees from the University of Electronic Science and Technology of China (UESTC), Chengdu, China, in 2015 and 2018, respectively.

He is currently an Associate Research Fellow with the School of information and Communication Engineering, UESTC. His research interests include array signal processing, MIMO radar waveform design, one-bit signal processing, and optimization theory.

ZISHU HE (Member, IEEE) was born in Chengdu, Sichuan, China, in 1962. He received the B.S., M.S., and Ph.D. degrees in signal and information processing from the University of Electronic Science and Technology of China (UESTC), in 1984, 1988, and 2000, respectively.

He is currently a Professor with the School of Electronic Engineering, UESTC. He has finished more than two hundred articles and has written two books. His current research interests include involved in array signal processing, digital beam forming, the theory on MIMO radar, and adaptive signal processing.